Polymer 53 (2012) 4033–4044

Contents lists available at SciVerse ScienceDirect

Polymer

journal homepage: www.elsevier.com/locate/polymer

Synthesis, morphology and properties of segmented poly(ether ester amide)s comprising uniform glycine or β-alanine extended bisoxalamide hard segments

Niels J. Sijbrandi [a], Ad J. Kimenai [b], Edwin P.C. Mes [b], René Broos [b], Georg Bar [c], Martin Rosenthal [d], Yaroslav I. Odarchenko [d], Dimitri A. Ivanov [d], Jan Feijen [a], Pieter J. Dijkstra [a,*]

[a] Department of Polymer Chemistry and Biomaterials, MIRA Institute for Biomedical Technology and Technical Medicine, Faculty of Science and Technology, University of Twente, P.O. Box 217, 7500 AE Enschede, The Netherlands
[b] Core R&D, Dow Benelux BV, P.O. Box 48, 4530 AA Terneuzen, The Netherlands
[c] Dow Olefin Verbund GmbH, P.O. Box 1163, D-06258, Schkopau, Germany
[d] Institut de Sciences des Matériaux de Mulhouse-IS2M, CNRS LRC 7228, Jean Starcky, 15, F-68057 Mulhouse, France

ARTICLE INFO

Article history:
Received 29 February 2012
Received in revised form
21 June 2012
Accepted 8 July 2012
Available online 27 July 2012

Keywords:
Thermoplastic elastomers
Segmented poly(ether ester amide)s
Oxalamides

ABSTRACT

Segmented poly(ether ester amide)s comprising glycine or β-alanine extended bisoxalamide hard segments are highly phase separated thermoplastic elastomers with a broad temperature independent rubber plateau. These materials with molecular weights, M_n, exceeding 30×10^3 g mol^{-1} are conveniently prepared by polycondensation of preformed bisester–bisoxalamides and commercially available PTHF diols. FT-IR revealed strongly hydrogen bonded and highly ordered bisoxalamide hard segments with degrees of ordering between 73 and 99%. The morphology consists of fiber-like nano-crystals randomly dispersed in the soft polymer matrix. The micro-structural parameters of the copolymers were addressed by simultaneous small- and wide-angle X-ray scattering. It is shown that the crystals have strictly identical thickness, which is close to the contour length of the hard segment. The long dimension of the crystals is identified with the direction of the hydrogen bonds. The melting transitions of the hard segments are sharp, with temperatures up to 170 °C. The studied polymers have an elastic modulus in the range of 139–170 MPa, a stress at break in the range of 19–31 MPa combined with strains at break of higher than 800%. The segmented copolymer comprising the β-alanine based bisoxalamide hard segment with a spacer of 6 methylene groups has a melting transition of 141 °C which is higher than the melting transition of its glycine analogue of 119 °C. Likewise, the fracture stress increased from 22 to 31 MPa when the glycine ester group in the hard segment was replaced with β-alanine. The improved thermal and mechanical properties of the latter polymers is related to the crystal packing of the β-alanine based hard segments in the copolymer compared to the packing of the hard segments comprising glycine ester groups.

1. Introduction

Segmented block copolymers consisting of alternating flexible soft segments and rigid hard segments are thermoplastic elastomers [1,2]. As a result of their phase separated morphology, these materials show elastomeric behavior at ambient temperatures and can be processed from solution or by heating the materials above the vitrification (in case of amorphous block copolymers) or melting point (in case of semi-crystalline block copolymers) of the hard domains. At ambient temperatures, the hard segments form rigid domains in a continuous matrix of soft segments [3]. These domains act as physical crosslinks providing stiffness and strength to the material. The properties of these segmented block copolymers are significantly affected by the symmetry, nature of hydrogen bonding and size distribution of the hard segment [4–18]. Symmetrical and uniform hard segments in segmented copolymers can easily crystallize and high degrees of crystallinity can be obtained. Consequently, copolymers with such segments usually have broad and temperature independent rubber plateaus, relatively high moduli and good ultimate mechanical properties.

Segmented block copolymers with uniform amide based hard segments have been prepared by Gaymans and coworkers [12,19–33]. The main two hard segments which have been used are the di-amide segment (TΦT) based on 1.5 repeating unit poly(p-phenylene terephthalamide) and the tetra-amide segment based on 2.5 repeating unit nylon-6,T (T6T6T). The corresponding segmented copolymers have been generally prepared by first

* Corresponding author. Tel.: +31 53 4893004; fax: +31 53 4892155.
E-mail address: p.j.dijkstra@utwente.nl (P.J. Dijkstra).

0032-3861/$ – see front matter © 2012 Elsevier Ltd. All rights reserved.
http://dx.doi.org/10.1016/j.polymer.2012.07.015

purifying the aromatic amide group containing monomers and subsequently reacting these monomers with polyether prepolymers in a two step solution/melt polymerization. Although the hard segments are relatively short, they crystallize fast and almost completely in the segmented copolymer. TEM and AFM analysis of these copolymers show a morphology of fiber-like nano-crystals randomly dispersed in a soft polymer matrix [19,20,33]. Even at a hard segment concentration of ~3 wt%, the polymers show a distinct phase separated morphology and hence good elastomeric and mechanical properties [20,27].

In our previous work, we prepared fully aliphatic segmented poly(ether amide)s based on uniform rigid oxalamide segments and flexible PTHF segments and studied their properties [34]. Copolymers comprising hard segments with two or three oxalamide units appear highly phase separated materials resulting in strong elastic materials. The oxalamide containing hard segments are strongly hydrogen bonded and highly ordered, forming fiber-like nano-crystals which are randomly dispersed in a soft polymer matrix. The flow temperatures of bisoxalamide based segmented poly(ether amide)s increased from 150 to 200 °C when the number of methylene groups between the two oxalamide groups was decreased from 10 to 2, but the melting transitions remained very broad. Copolymers with three oxalamide groups in the hard segment had a flow temperature of 220 °C. The use of hard segments with either two or three oxalamide groups provided materials with attractive mechanical properties. Due to the high flow temperatures of the copolymers with three oxalamide groups in the hard segment, melt processing of these materials becomes difficult. Therefore, poly(ether amide)s composed of hard segments containing two oxalamide groups seem to give the optimum balance between the materials properties and processability.

The bisoxalamide based segmented poly(ether amide)s were previously prepared by first reacting bis(3-aminopropyl) end functionalized polytetrahydrofuran with an excess of diethyl oxalate [34]. Subsequently, the amide–ester capped polytetrahydrofuran soft segment was polycondensated in the melt with a linear aliphatic α,ω-diamine chain extender. Although the synthesis of these polymers is straightforward, α,ω-diamine end functionalized prepolymers are needed. In general, the commercial availability of such prepolymers is limited and/or they are relatively expensive. In contrast, a wide range of α,ω-hydroxyl end functionalized prepolymers (high molecular weight diols) are commercially available or synthetically easily accessible, some may have a renewable origin. Therefore, a more attractive strategy to prepare bisoxalamide based segmented block copolymers is the polycondensation of α,ω-hydroxyl end functionalized prepolymer soft segments with preformed OH reactive bisester–bisoxalamide hard segments.

To explore this new strategy, we have prepared segmented copolymers based on polytetrahydrofuran diol soft segments and hard segments containing two oxalamide groups, in which these groups are separated by spacers with different lengths. Moreover the hard segments were either terminated by a glycine or a β-alanine ester residue (industrial amino acids) to make those OH reactive. The molecular weight (M_n) of the soft PTHF segment was varied from 1.0×10^3 to 2.9×10^3 g mol^{-1}. The influence of the structure of the hard segment and the M_n of the soft PTHF block on the properties of the resulting copolymers was evaluated.

2. Experimental

The synthesis and characterization of the bisester-bisoxalamide monomers and corresponding segmented poly(ether ester amide)s are described in the Supplementary Information.

2.1. NMR

^{1}H (300 MHz) and ^{13}C NMR (75.26 MHz) spectra were recorded on a Varian Inova Nuclear Magnetic Resonance Spectrometer using $CDCl_3$-d_1 and TFA-d_1 as solvents.

2.2. GPC

The GPC setup consisted of a Perkin Elmer series 200 binary pump, a Perkin Elmer series 200 autosampler, a Shimadzu CTO-AVP column oven, and a Shimadzu RID-10A refractive index detector. The eluent was $CHCl_3$/HFIP (95/5 v/v). The flow was set at 1 ml min^{-1}. The injection volume was 200 μl. The separation was performed on two PL Mixed-D columns (300 × 7.5 mm) from Polymer Laboratories Ltd., packed with 5 μm particles. The temperature of the columns was set at 30 °C. Approximately 120 mg of sample was weighed in a 50 ml vial. To this vial 2 ml of HFIP was added and the solution is allowed to stand for 2 h. Next, 38 ml of warm (~35 °C) HPLC-quality chloroform was added and mixed thoroughly. Prior to injection, the sample solution was filtered through a Millex-LCR 0.45 μm filter (Millipore). The system was calibrated with 14 narrow polystyrene standards (Polymer Laboratories) with MW ranging from 5.8×10^2 to 1.0×10^6 g mol^{-1}. The standards were dissolved in $CHCl_3$/HFIP (95/5 v/v). Because the K and α values of the samples are not known and a viscometer was not available, no universal calibration could be performed. The reported molecular weights should, therefore, be regarded as PS-equivalent molecular weights. A calibration curve that is virtually linear over a broad molecular weight range was obtained. However, the three highest molecular weights tested (6.75×10^5 g mol^{-1}, 8.41×10^5 g mol^{-1}, and 1.0×10^6 g mol^{-1}) elute near or in the exclusion limit of the column, causing an upward curvature at the high MW end.

2.3. FT-IR

To minimize the potential oxidation of the material, sample preparation comprised the following steps. The surface of a 32 × 3 mm NaCl disc (Thermo, International Crystal Labs) was roughened to prevent interfering fringes. Subsequently, a polymer solution of 0.3–0.5 g ml^{-1} in dichloromethane was drop casted on the NaCl disk and the solvent was allowed to evaporate. This step was repeated until the polymer film thickness gave a maximum peak height of 0.5–0.7. The holder was placed in the cell in an inert atmosphere (N_2 purge glove bag or N_2 purged IR sample compartment). The cell was heated to 20–50 °C above the T_m of the polymer and subsequently cooled to room temperature. Fourier transform infra-red spectra were recorded on a Thermo 5700 spectrometer utilizing a DTGS detector at 4 cm^{-1} resolution. The temperature of the prepared polymer film was controlled by an infra-red cell from Spectra Tech (model 0019-019). The data were collected between 4000 and 500 cm^{-1} (16 scans were acquired). The graphs were prepared using OPUS 6.1 software. All spectra were normalized to the 2860 cm^{-1} signal. The carbonyl region was analysed quantitatively in terms of free, bonded and ordered amide structures by curve fitting (Omnic version 7.2) and following the guidelines of Meier et al. [35].

2.4. DSC

Thermal analysis was carried out using a Perkin–Elmer Pyris 1. Calibration was carried out with pure indium. Samples (5–10 mg) were heated from −100 to 200 °C at a rate of 20 °C min^{-1}, annealed for 5 min, cooled to −100 °C at a rate of 20 °C min^{-1}, and subsequently heated from −100 to 200 °C at a rate of 20 °C min^{-1}. Melting (T_m) and crystallization (T_c) temperatures were obtained from the peak maxima, melting (ΔH_m) and crystallization (ΔH_c)

enthalpies were determined from the area under the curve. The data presented are taken from the first cooling scan and the second heating scan.

2.5. TGA

Thermal gravimetric analysis was carried out with 5–10 mg samples under a nitrogen atmosphere in the 50–700 °C range at a heating rate of 10 °C min^{-1}, using a Perkin–Elmer Thermal Gravimetric Analyser TGA 7.

2.6. AFM

Atomic force microscopy images were obtained using a Multi-Mode scanning probe microscope (SPM) (Veeco Metrology Group, Santa Barbara, CA) with a Nano-Scope IV controller running software version 5.12. The TESP probe used was 125 μm in length, had a tip radius of 8 nm and a force constant of 40 N m^{-1}. A moderate tapping ratio of about 0.5 was applied in all measurements. Height and phase images were recorded at various magnifications. Samples were prepared by drop casting a 1 mg ml^{-1} chloroform solution on a silicon waver. After evaporation, the sample was heated to 20 °C above the T_{flow} for 15 min and slowly cooled to room temperature.

2.7. X-ray scattering

Wide- (WAXS) and small-angle X-ray scattering (SAXS) measurements were performed on the BM26 beamline of the ESRF (Grenoble, France) using the wavelength of 1.04 Å. The experimental setup comprised a FReLoN detector mounted on a motorized stage, which ensured adjustable sample-to-detector distance and allowed to record the signal in the s-range ($s = 2\sin\theta/\lambda$, where θ is the Bragg angle) from 0.01 to 0.5 $Å^{-1}$. The modulus of the scattering vector s was calibrated using several diffraction orders of silver behenate in both setups. The patterns were collected in transmission geometry. The sample temperature was controlled by a Linkam heating stage.

To estimate the chain tilt in the hard-block crystals the copolymer films were oriented by drawing them (draw ratio 300%). The taut films were fixed with the help of a metal frame and then directly used for X-ray scattering measurements.

2.8. Processing

Compression molded bars (75 × 10 × 2 mm) were prepared using a hot press (THB 008, Fontijne Holland BV, the Netherlands). Polymers were heated for 4 min at approximately 20 °C above their T_{flow}, pressed for 3 min at 300 kN, and cooled in approximately 5 min under pressure to room temperature.

2.9. DMA

Dynamic mechanical analysis was performed using a Myrenne ATM3 torsion pendulum at a frequency of approximately 1 Hz. The storage modulus (G′) and the loss modulus (G″) were measured as a function of temperature. Samples (50 × 10 × 2 mm) were cooled to −100 °C and then heated at a rate of 1 °C min^{-1}. The temperature at which the loss modulus reached a maximum was taken as the glass transition temperature (T_g). The flow temperature (T_{flow}) was taken at a storage modulus value of 1 MPa.

2.10. Tensile testing

Tensile tests were conducted with compression molded bars cut to dumbbells (ISO37 type 2). A Zwick Z020 universal tensile machine equipped with a 500 N load cell and extensometers was used to measure the stress at a strain rate of 0.4 s^{-1} (test speed: 60 mm min^{-1}) and a preload of 0.1 MPa. Measurements were performed on at least 5 different polymer bars.

3. Results & discussion

3.1. Synthesis

The synthesis of symmetrical bisoxalamides **2a**–**c** and **3** capped with glycine ethyl ester or β-alanine ethyl ester groups is depicted in Scheme 1. First, bisoxalamide precursors **1a**–**c** were prepared by

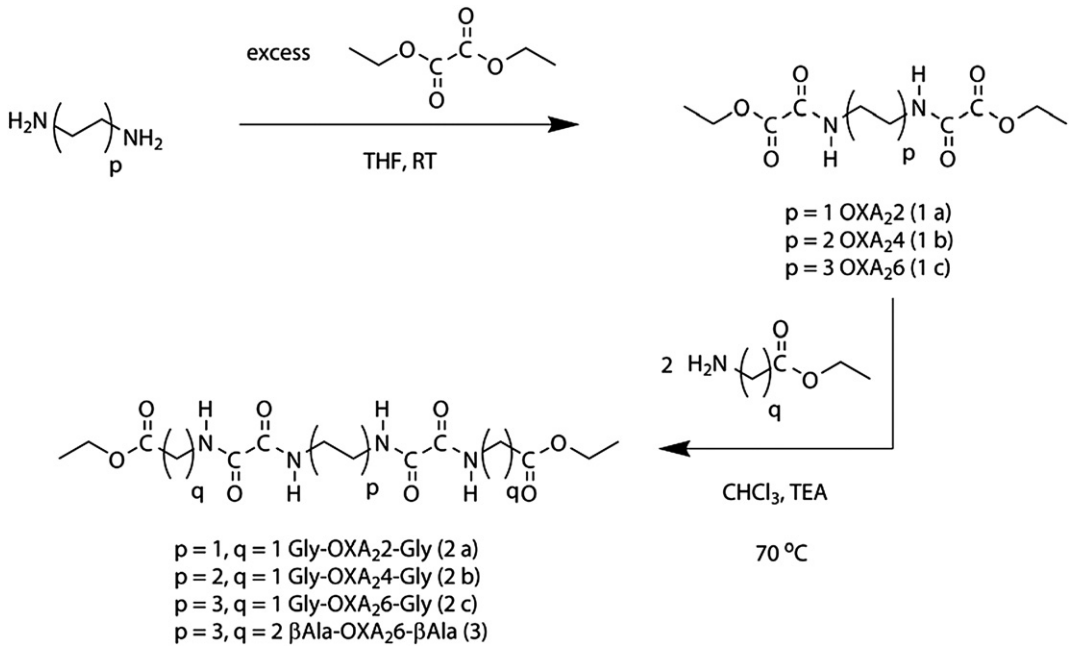

Scheme 1. Synthesis of bisester–bisoxalamide monomers (**2a**–**c**, **3**).

reacting α,ω-diamine spacers with an excess of diethyl oxalate. The compounds were obtained in good yields after purification. The ^{1}H and ^{13}C NMR analysis of the crude products revealed the formation of small amounts of oligomers, which were removed by selective extraction with chloroform. Reaction of **1a–c** with glycine ethyl ester afforded the bisester–bisoxalamides **2a–c**. Similarly, **3** was prepared from **1c** upon reaction with β-alanine ethyl ester. The ^{1}H NMR spectra of the products revealed a high purity of **2a–c** and **3** by comparing the integral values of the glycine or β-alanine methylene protons with the central methylene protons next to the amide groups. Side reactions, like the reaction of **2a** with glycine ethyl ester, were not observed as ^{13}C NMR spectral data showed no carbonyl peaks found at $\delta = 178$ characteristic of single amides [36].

The segmented poly(ether ester amide)s were prepared by melt polycondensation of α,ω-hydroxyl end functionalized polytetrahydrofuran (PTHF diols) **4a–c** (1.0×10^3, 2.0×10^3 and 2.9×10^3 g mol^{-1}) and bisester–bisoxalamides **2a–c** and **3** (Scheme 2). The condensation reactions of PTHF-Gly-OXA$_2$6-Gly **(7a–c)** were performed at 250 °C and low pressure for 3 h. The polymers were obtained as yellow elastic transparent solids in high yields. To prevent thermal degradation, which was observed during polycondensation of PTHF$_{1000}$-Gly-OXA$_2$2-Gly **(5)** at 250 °C, the synthesis of polymers **5**, **6** and **8** was performed in a slightly different way. First, the reaction mixture was heated to a temperature of approximately 230 °C. When the melt was transparent, the temperature was decreased to 190 °C and the reaction was continued for 3 h at low pressure. Also these materials were obtained as transparent elastic solids and their color changed from yellow **(5)** to colorless for polymers **6** and **8**. ^{1}H NMR analysis revealed the absence of ethyl ester or hydroxyl end groups indicating relatively high molecular weights. GPC analysis confirmed molecular weight values between 34×10^3 and 83×10^3 g mol^{-1} and polydispersity indices (PDI's) of 2–3 relative to polystyrene standards (Table 1). The somewhat higher PDI values for **7a–c** from GPC analysis may be ascribed to the solubility of the polymers in a mixture of 1,1,1,3,3,3-hexafluoro-2-propanol and chloroform resulting in tailing towards the high molecular weight end.

Table 1
Molecular weights of segmented poly(ether ester amide)s **5-8**.

	Content[a]		M_n (g mol^{-1} $\times 10^3$)	PDI (−)
	Soft Segment (wt%)	Hard Segment (wt%)		
PTHF$_{1000}$-Gly-OXA$_2$6-Gly **(7a)**	74.6	25.4	42	3.3
PTHF$_{2000}$-Gly-OXA$_2$6-Gly **(7b)**	85.5	14.5	62	2.7
PTHF$_{2900}$-Gly-OXA$_2$6-Gly **(7c)**	89.5	10.5	83	2.7
PTHF$_{1000}$-Gly-OXA$_2$2-Gly **(5)**	77.8	22.2	34	2.0
PTHF$_{1000}$-Gly-OXA$_2$4-Gly **(6)**	76.2	23.8	52	1.9
PTHF$_{1000}$-βAla-OXA$_2$6-βAla **(8)**	73.1	26.9	59	1.9

[a] The ester groups are included in the calculation of the hard segment content.

3.2. FT-IR

The FT-IR spectra of the segmented poly(ether ester amide)s with varying hard segments **(5–8)** are presented for the selected wave number regions 3500–2700 and 1800–1400 in Fig. 1. Characteristic IR bands are found at ~3295 (Amide A, ν N–H, H-bonded), 1736–1746 (ν C=O ester, non H-bonded), ~1650 (Amide I, ν C=O amide, H-bonded ordered), ~1530 cm^{-1} (Amide II, ν C–N + δ N–H) (Table 2).

For all polymers, the N–H and C=O stretching vibrations appear as sharp bands at 3295 and 1650 cm^{-1}, respectively. This indicates that the bisoxalamide segments in the polymers are highly ordered and strong hydrogen bonds are formed between the oxalamide groups. These observations suggest a high degree of phase separation and the presence of at least paracrystalline amide domains

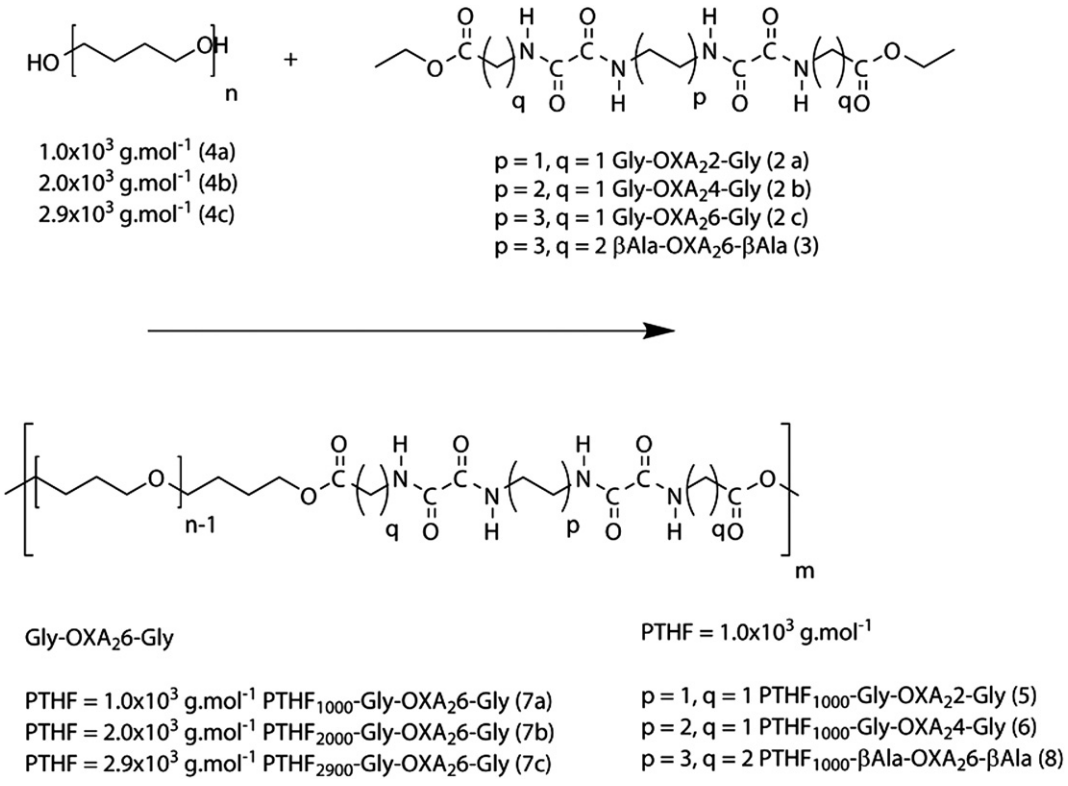

Scheme 2. Synthesis of segmented poly(ether ester amide)s **5–8**.

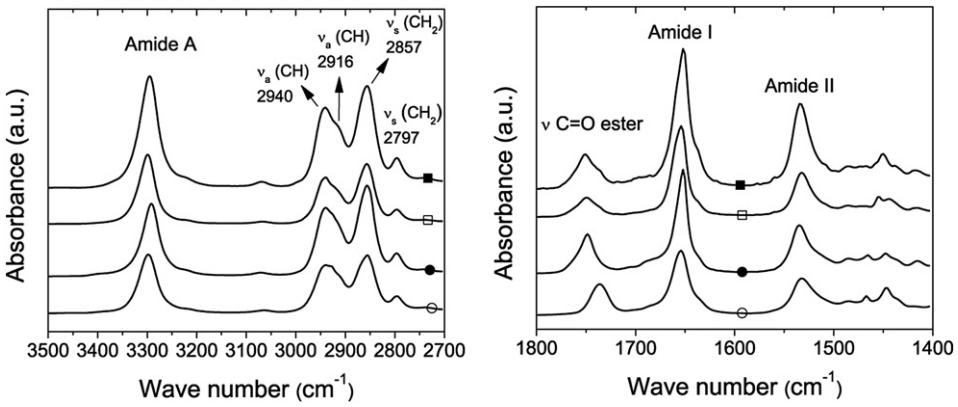

Fig. 1. FT-IR spectra of segmented poly(ether ester amide)s (■) $PTHF_{1000}$-Gly-$OXA_2$2-Gly at 40 °C **(5)**, (□) $PTHF_{1000}$Gly-$OXA_2$4-Gly at 30 °C **(6)**, (●) $PTHF_{1000}$-Gly-$OXA_2$6-Gly at 35 °C **(7a)** and (○) $PTHF_{1000}$-βAla-$OXA_2$6-βAla **(8)** at 50 °C.

Table 2
Thermal properties of segmented poly(ether ester amide)s **5**–**8**.

	T_d (°C)	T_g (°C)	Hard segment				T_{onset} (°C)	Super cooling (°C)	X_c[a] (%)
			T_m (°C)	ΔH_m (J g^{-1})	T_c (°C)	ΔH_c (J g^{-1})			
7a	420	−68	119	25	88	23	99	20	85
7b	426	−76	116	16	83	16	96	20	95
7c	426	−75	111	12	80	11	91	20	99
5	393	−74	171	28	159	26	166	5	100
6	406	−73	138	29	109	29	122	16	100
8	421	−70	46/142	5/28	13/125	5/32	129	13	88

[a] Degree of crystallinity determined by DSC.

formed by association or stacking of bisoxalamide arrays. Importantly, the ester C═O stretching vibration band of the glycine **(5**, **6** and **7a)** and β-alanine **(8)** moieties in the segmented poly(ether ester amide)s are found at 1746 and 1736 cm^{-1}, respectively, indicative of non-hydrogen bonded ester groups. These wave numbers are similar to those found for the monomers **2a**–**c** and **3** and point to a similar crystalline structure of the monomer and the hard segments in the polymer (see Fig. S-1 in Supplementary Information). Moreover, this observation suggests that the ester carbonyl groups are spatially tilted away from the oxalamide plane. The higher wave number of the glycine ester carbonyl compared to the β-alanine ester carbonyl vibration band is likely due to rotation of the former group into a more a-polar surrounding.

The amide II band, which is especially sensitive to polymorphism resulting from differences in chain conformation, like the α- or γ-crystalline structures of nylons, is located at ~1532 cm^{-1} for all four polymers. Previous research on segmented poly(ether amide)s with bisoxalamide hard segments showed a similar position of the amide II band for spacer lengths of 2 and 4 methylene groups, but this position shifted to ~1520 cm^{-1} for bisoxalamides with spacer lengths of 6 methylene groups and higher [34]. Higher wave numbers for bisoxalamide segments with decreasing spacer length can be attributed to increasing chain distortions and hence deviations from the fully extended zig-zag conformation. The amide II position of the segmented poly(ether ester amide)s with bisoxalamide segments having spacer lengths of 6 methylene groups is located at ~1532 cm^{-1}, whereas the amide II position of the corresponding segmented poly(ether amide) is found at a wave number of 1520 cm^{-1}. Apparently, the glycine and β-alanine ester groups induce a tilting of the oxalamide groups from a fully extended planar zig-zag conformation thereby shifting the amide II band to higher wave numbers.

The effect of temperature on the extent of hydrogen bonding and organization of the hard segment was studied with temperature dependent FT-IR. The N–H stretching vibration band and ester and amide C═O stretching vibration bands of $PTHF_{1000}$-Gly-$OXA_2$6-Gly **(7a)** at different temperatures are depicted in Fig. 2. This polymer had a sharp melting transition between 105 and 135 °C (*vide infra*, Thermal Properties, DSC). Between 100 and 140 °C the hydrogen bonded amide N–H vibration band shifts from 3292 to

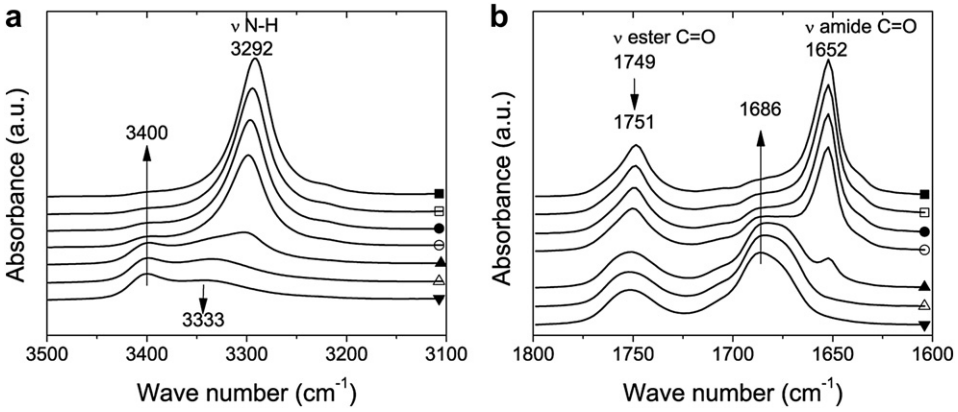

Fig. 2. FT-IR spectra of $PTHF_{1000}$-Gly-$OXA_2$6-Gly **(7a)** at 35 ■, 70 □, 100 ●, 120 ○, 140 ▲, 170 Δ and 200 °C ▼ for (a) the N–H stretching vibration band and (b) the ester and amide C═O stretching vibration band.

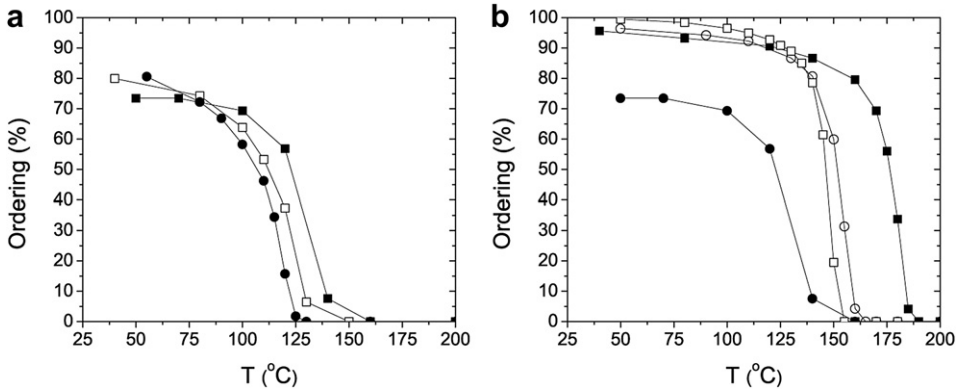

Fig. 3. Hard segment ordering as a function of the temperature for (a) (■) $PTHF_{1000}$-Gly-$OXA_2$6-Gly **(7a)**, (□) $PTHF_{2000}$-Gly-$OXA_2$6-Gly **(7b)** and (●) $PTHF_{2900}$-Gly-$OXA_2$6-Gly **(7c)**. (b) (■) $PTHF_{1000}$-Gly-$OXA_2$2-Gly **(5)**, (□) $PTHF_{1000}$-Gly-$OXA_2$4-Gly **(6)**, (●) $PTHF_{1000}$-Gly-$OXA_2$6-Gly **(5a)** and (○) $PTHF_{1000}$-βAla-$OXA_2$6-βAla **(8)**.

Table 3
Long spacing (LB), crystalline lamellar thickness (L_c and D) and amorphous lamellar thickness (L_a) of segmented poly(ether ester amide)s **5**–**8**.

	L_B (Å)	L_c (Å)	D (Å)	L_a (Å)	Chain tilt (deg)	Stem length[a] (Å)	Hard block length[b] (Å)
7a	57.5	24	32	33.5	~5–10	24	18.75
7b	71.4	24	27	47.4	~5–10	24	18.75
7c	79	24	24	55	~5–10	24	18.75
5	49.8	14.3	29	35.5	~5–10	14.5	13.75
6	52.6	17.4	32	35.2	~5–10	17.6	16.25
8	73	22.9	50	50.1	~28	25	18.75

[a] The value obtained by dividing L_c by the cosine of the tilt angle.
[b] The hard block length is defined as a part of the molecule delimited by the hydrogen bonds.

3333 cm^{-1} and broadens, indicating that the strength of the hydrogen bonds decreases (Fig. 2a). In addition, a new band at 3400 cm^{-1} characteristic of free N–H bonds arises. Melting of the hard segments is also reflected by the strong decrease of the H-bonded ordered amide C=O stretching vibration band at 1652 cm^{-1} and the appearance of the non H-bonded amide C=O peak at 1686 cm^{-1} (Fig. 2b). Such observation seems to agree with the disruption of a crystalline type of order. The ester C=O stretching vibration at 1749 cm^{-1} only slightly broadens and decreases in intensity as expected for non-ordered and non hydrogen-bonded ester groups. Similar structural characteristics were observed in the FT-IR spectra of the segmented poly(ether ester amide)s **5, 6** and **8**.

The degree of hard segment organization can be estimated by deconvolution of the amide C=O stretching band and calculation of the ratio of the area associated with the hydrogen bonded ordered amide phase at 1652 cm^{-1} to the total amide absorption area. For the polymers comprising Gly-$OXA_2$6-Gly hard segments **7a**–**c**, the molar fraction of ordered hard segments ranged from 73 to 85%, while this value was between 95 and 100% for polymers $PTHF_{1000}$-Gly-$OXA_2$2-Gly **(5)**, $PTHF_{1000}$-Gly-$OXA_2$4-Gly **(6)** and $PTHF_{1000}$-βala-$OXA_2$6-βAla **(8)**. The hard segment ordering of these polymers as a function of the temperature is depicted in Fig. 3. By increasing the M_n of the polytetrahydrofuran soft segment and thus decreasing the hard segment content, the process of relative reduction in ordered H-bonded amide species shifts to slightly lower temperatures (Fig. 3a). This can be explained by the solvent effect proposed by Flory [37]. Upon dilution of the ordered hard segments by increasing the molar fraction of the soft segment, the size of the ordered domains will become smaller. The melting transitions observed appeared more affected by changing the number of methylene groups between the oxalamide moieties. Increasing the number of methylene groups in the spacer connecting the two oxalamide moieties shifted the transition to lower temperatures. Replacing the glycine end-functional group by β-alanine however shifted the transition to a higher temperature. This may be explained by a better packing of the β-alanine end groups in the structure.

3.3. Thermal properties

The crystallization and melting temperatures and corresponding enthalpies of the segmented poly(ether ester amide)s were

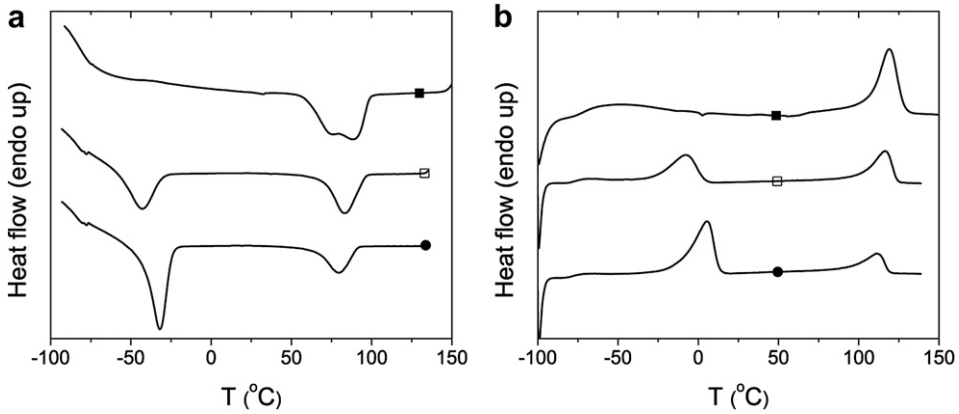

Fig. 4. DSC first cooling curves (a) and second heating curves (b) of segmented poly(ether ester amide)s (■) $PTHF_{1000}$-Gly-$OXA_2$6-Gly **(7a)**, (□) $PTHF_{2000}$-Gly-$OXA_2$6-Gly **(7b)** and (●) $PTHF_{2900}$-Gly-$OXA_2$6-Gly **(7c)**.

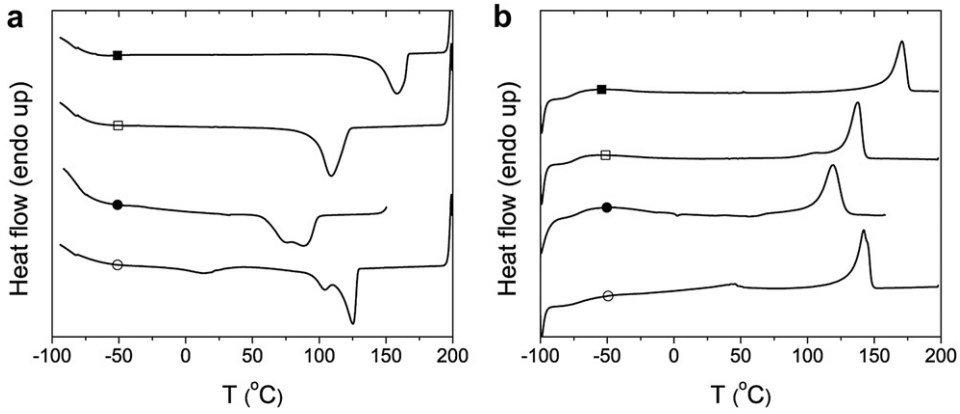

Fig. 5. DSC first cooling curves (a) and second heating curves (b) of segmented poly(ether ester amide)s (■) $PTHF_{1000}$-Gly-$OXA_2$2-Gly **(5)**, (□) $PTHF_{1000}$-Gly-$OXA_2$4-Gly **(6)**, (●) $PTHF_{1000}$-Gly-$OXA_2$6-Gly **(7a)** and (○) $PTHF_{1000}$-βAla-$OXA_2$6-βAla **(8)**.

taken from the first cooling scan and the second heating scan as measured by DSC (Table 3).

The segmented poly(ether ester amide)s exhibit a glass transition temperature between −68 and −76 °C. The DSC curves displayed in Fig. 4 show the effect of the soft segment M_n on the thermal properties. $PTHF_{1000}$-Gly-$OXA_2$6-Gly **(7a)** has a melting transition at 119 °C and a crystallization transition at 99 °C. Increasing the polytetrahydrofuran monomer segment M_n from 2.0×10^3 to 2.9×10^3 g mol^{-1}, results in an additional thermal transition, which is attributed to crystallization of the soft polytetrahydrofuran phase. The melting temperature increases from −9 to −5 °C and the crystallization temperature increases from −43 to −32 °C with increasing polytetrahydrofuran M_n. Contrary, the melting temperature of the bisoxalamide phase decreases from 119 to 111 °C as the polytetrahydrofuran M_n increases and thus the hard segment content decreases.

The effect of the number of methylene units separating the bisoxalamide moieties in the hard segment on the polymer thermal properties is depicted in Fig. 5. The segmented poly(ether ester amide)s comprising glycine based bisoxalamide hard segments **5**, **6** or **7a** show one melting and crystallization transition attributed to the bisoxalamide hard segment crystals. By increasing the number of methylene groups from 2 to 6, the melting temperature decreases from 171 to 119 °C. This trend is generally observed for nylon type materials, which show a decrease in melting temperature when the amide-to-methylene ratio decrease *i.e.* when the concentration of hydrogen bonds in the polymer chain decreases. The melting temperature of the polymer made with the β-alanine capped hard segment **(8)** is found at 142 °C, which is much higher than that of its glycine analogue **7a** (119 °C). A similar phenomena is observed for the bisester-bisoxalamide monomers Gly-$OXA_2$6-Gly **(2c)** (181 °C) and βAla-$OXA_2$6-βAla **(3)** (196 °C) (see Fig. S-2 in Supplementary Information).

The degree of hard segment crystallinity in the polymer was calculated by using the melting enthalpies determined for the monomers (see Table S-2 in Supplementary Information). For all polymers, the crystallinity of the amide phase is higher than 85% (Table 3). The super cooling effect, the difference between the melting temperature and the crystallization onset, is for all polymers lower than 20 °C consistent with fast crystallization of the hard segments, which is favorable for processing.

Thermal stability of the segmented poly(ether ester amide)s **5**–**8** under non-oxidative conditions was investigated by thermal gravimetric analysis (TGA). The segmented poly(ether ester amide)

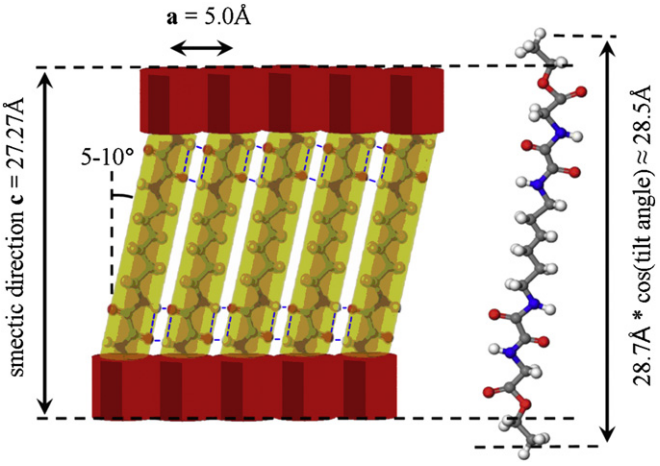

Fig. 6. Sketch of the crystalline structure of the model compound Gly-$OXA_2$6-Gly **(2c)**.

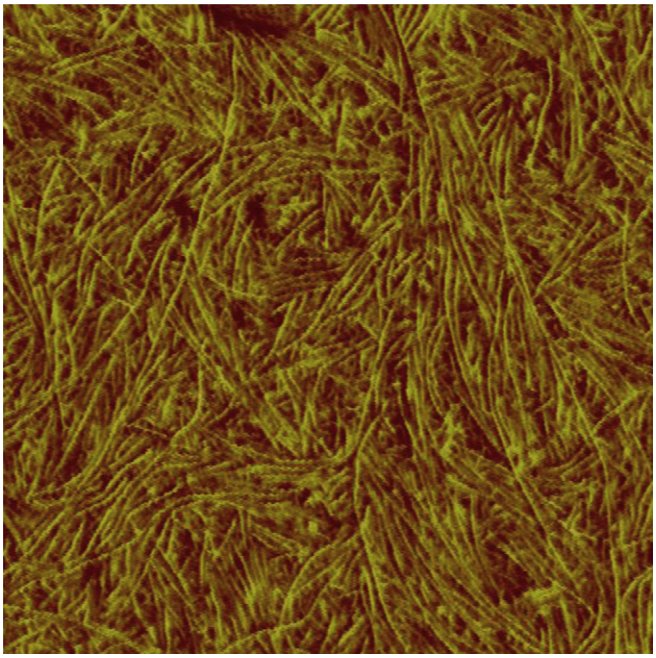

Fig. 7. Phase image of $PTHF_{1000}$-βAla-$OXA_2$6-βAla **(7)** (image size: 1 × 1 μm).

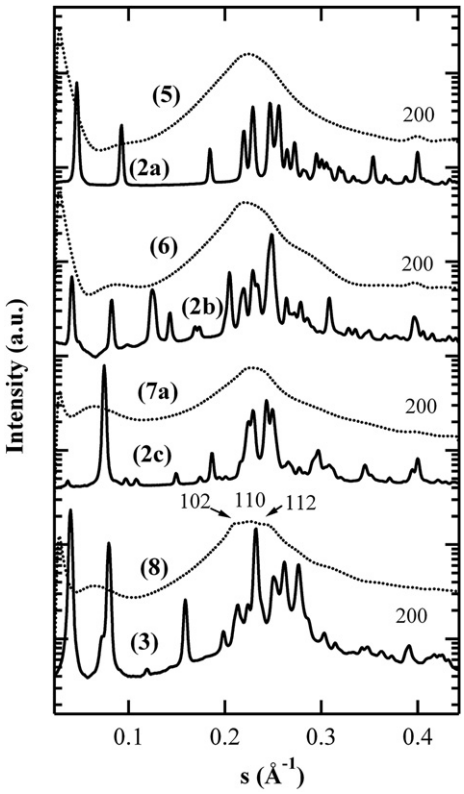

Fig. 8. WAXD curves of bisester-bisoxalamide monomers and corresponding copolymers of Gly-$OXA_2$2-Gly **(2a)** and $PTHF_{1000}$-Gly-$OXA_2$2-Gly **(5)**, Gly-$OXA_2$4-Gly **(2b)** and $PTHF_{1000}$-Gly-$OXA_2$4-Gly **(6)**, Gly-$OXA_2$6-Gly **(2c)** and (d) $PTHF_{1000}$-Gly-$OXA_2$6-Gly **(7a),** βAla-$OXA_2$6-βAla **(3)** and $PTHF_{1000}$-βAla-$OXA_2$6-βAla **(8)**.

s are stable up to ~390 °C (Table 3). For all polymers, the decomposition temperatures are considerably higher than the melting temperature, which is important for processing of the materials.

3.4. Morphology

In our previous study [34], we suggested that bisoxalamide hard segments in segmented poly(ether amide)s form fiber-like nanocrystals as schematically depicted in Fig. 9a. It was shown that the long direction of the crystals is the direction of the hydrogen bonds (***a***-direction). In the present work, we explore the structure of segmented poly(ether ester amide)s based on glycine or β-alanine extended bisoxalamide hard segments **(5–8)**. As mentioned previously, the copolymers are phase separated into relatively pure amide and polyether domains. FT-IR measurements accordingly revealed that the bisoxalamide-based hard segments are highly ordered and that hydrogen bonds are solely formed between the oxalamide groups. This leads to a picture of bisoxalamide crystalline structures formed by a process of self-assembly of oxalamide groups into hydrogen bonded sheets with subsequent stacking of the hydrogen bonded sheets. The crystalline structure of the hard segments likely resembles the crystalline structure of the corresponding monomers **2a–c** and **3**, and was addressed by X-ray diffraction and FT-IR measurements (see Fig. S-3 In Supplementary Information).

Table 4
Dynamic mechanical properties of segmented poly(ether ester amide)s **5–8**.

	Content[a]		X_c[b](%)	T_g(°C)	$G'_{(25\ °C)}$(Mpa)	T_{flow}(°C)
	Soft segment (%)	Hard segment (%)				
7a	74.6	25.4	85	−70	55	122
7b	85.5	14.5	95	−75	28	117
7c	89.5	10.5	99	−75	12	112
5	77.8	22.2	100	−70	79	170
6	76.2	23.8	100	−70	79	137
8	73.1	26.9	88	−65	77	143

[a] The ester groups are included in the calculation of the hard segment content.
[b] Degree of crystallinity determined by DSC.

As example a sketch of the crystal structure of Gly-$OXA_2$6-Gly **(2c)** is shown in Fig. 6. The monomers form hydrogen bonded sheets by stacking of the bisoxalamide units forming like-to-like amide–amide hydrogen bonds with a hydrogen bonding distance of ~5 Å (***a***-direction). The calculated molecular length of **2c** is 28.75 Å whereas the ***c***-parameter is 27.27 Å. The tilt of the molecule with respect to the normal to the layers was addressed from X-ray patterns of the oriented copolymer (see Fig. S-5 In Supplementary Information). From the characteristic four-spot SAXS patterns it was found that the hard segment has a slight tilt of 5–10° i.e. the central part of the molecule is oriented almost perpendicular to the smectic planes. Consequently, the glycine and β-alanine carbonyl ester groups are probably tilted away from the oxalamide plane in order to accommodate the molecule within the layers of 27.27 Å

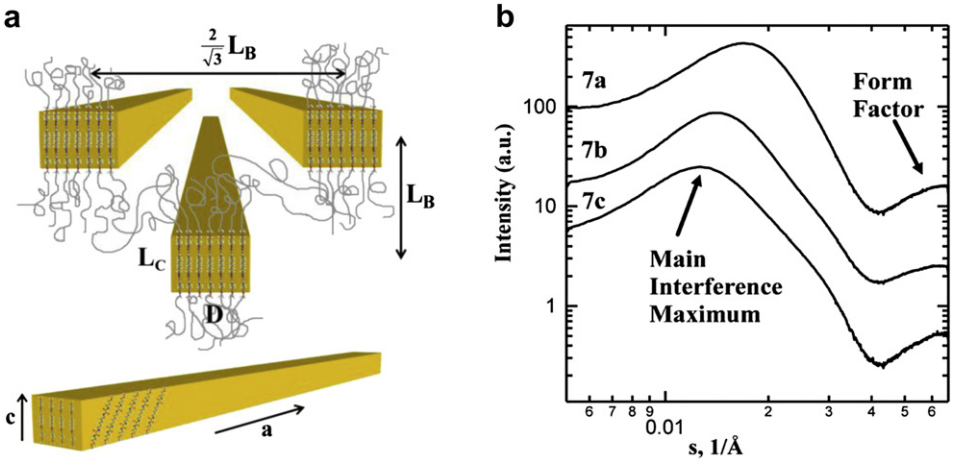

Fig. 9. (a) Fibrillar crystal model used for interpretation of the SAXS data [34]. (b) SAXS intensities corresponding to the segmented poly(ether ester amide)s consisting of Gly-$OXA_2$6-Gly **(2c)** hard segments and PTHF soft segments with varying lengths **(7a–c)**.

(Fig. 6). For all the studied compounds the distance between the hydrogen bonded sheets was ~5 Å (***b***-direction is normal to H-bonded sheets) (see Fig. S-4 In Supplementary Information).

To obtain more insight in the crystalline structure of the hard segments in the PEEAs, the materials were further investigated using AFM and X-ray diffraction techniques.

3.4.1. Atomic force microscopy

To illustrate the highly phase separated structure of the segmented poly(ether ester amide)s, the morphology was visualized with atomic force microscopy (AFM) (Fig. 7) The results reveal a morphology characterized by long ribbon-like nano-crystals in a soft polymer matrix. A similar morphology was shown in previous research for analogous bisoxalamide based segmented poly(ether amide)s [34].

The AFM measurements confirm the proposed fiber-like model as depicted in Fig. 9a. Because the AFM tip has a radius of 8 nm, an accurate determination of the fiber diameter (≤3 nm) was not possible. The length of the crystals is up to several hundreds of nanometers. However, the full length of the crystals cannot be determined since only the surface morphology of the sample is scanned.

3.4.2. WAXD

The diffraction peaks observed for the bisoxalamide monomers are largely absent from the curves of the corresponding copolymers and a broad amorphous halo originating from the PTHF phase is mainly visible for samples **5**–**7** (Fig. 8). The fact that the diffraction peaks are scarce in the patterns of the copolymers can be explained by the small crystal thickness along the ***c***-direction. Moreover, since only the 200 peak shows up in the WAXS curves for all polymers, it can be suggested that the small dimensions of the fibers are in the ***bc***-plane while the ***a***-parameter is parallel to the long fibrillar axis. However, the diffraction in the ***b***-direction, *i.e.* the direction of stacking of the hydrogen bonded sheets, is weak in the diffractogram of the corresponding monomers and consequently not visible in the X-ray pattern of the polymer. For copolymer **8** one can notice three maxima on top of the amorphous halo, which were indexed as 102, 110 and 112 of the orthorhombic unit cell with parameters $\boldsymbol{a} = 5.03$ Å, $\boldsymbol{b} = 11.03$ Å and $\boldsymbol{c} = 25.18$ Å.

3.4.3. SAXS

The SAXS curves of all segmented poly(ether ester amide)s **5**–**8** show an interference maximum indicative of the presence of phase separated domains. Based on the fibrillar morphology observed with AFM, the interpretation of the SAXS curves was done using a 2D structural model (Fig. 9a) [34]. Thus, it is assumed that the sample structure is composed of fiber-like crystals having a virtually infinite length. The long spacing (L_B), crystal (L_c) and amorphous domain thickness (L_a) are all derived from the SAXS curves (Fig. 9b).

The L_B is determined from the position of the Bragg peak whereas the crystalline domain thickness along the chain direction (L_c) was calculated from the position of the form factor (FF) described by the following expression:

$$A + \frac{B}{s^n}\left(\frac{\sin(\pi s L_c)}{(\pi s L_c)}\right)^2 \qquad (1)$$

where A, B, n are constants. It is noteworthy that the fact that the crystals' form factor is observed in SAXS curves signifies that the crystal thickness is rather monodisperse. For example, observation of the crystals' form factor constitutes a rare observation for semicrystalline polymers because variation of the crystallization temperature during the structure formation and structural defects of different nature easily suppress this feature from the SAXS curves [38–40]. In our case, the monodispersity of the crystals is determined by the chemistry of the copolymers and therefore should be independent from the crystallization conditions.

The characteristic crystal size D was calculated in the same way as in our previous work on segmented poly(ether amide)s [34]. The resulting long spacing (L_B), crystal dimensions (L_c and D) and amorphous layer thickness (L_a) are listed in Table 4. It can be seen that the L_B and the L_a increase with the increase of M_n of the PTHF segment length from 1.0×10^3 to 2.9×10^3 g mol^{-1} **(7a–c)**, whereas the crystal thickness L_c remains constant. This is logical because the weight fraction of the fibrillar crystals formed by the hard block is directly affected by the PTHF segment length. Another interesting observation is that L_a can significantly differ for the hard blocks with different end groups (cf. for example samples **7a** and **8**). This is linked to the variation of the crystal width, *i.e.* when the crystals become wider, the nearest neighbor distance increases accordingly. As far as the crystal thickness is concerned the value of L_c increases with the spacer length between oxalamide groups. Therefore the

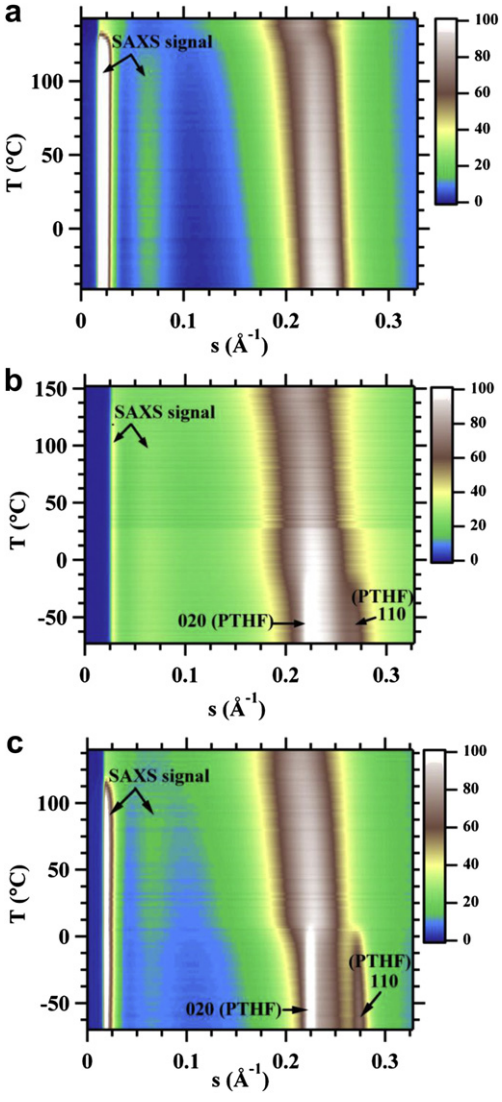

Fig. 10. Results of simultaneous SAXS/WAXS measurements performed during heating for segmented poly(ether ester amide)s with polytetrahydrofuran with molecular weights of (a) 1.0×10^3 g mol^{-1} **(7a)**, (b) 2.0×10^3 g mol^{-1} **(7b)** and (c) 2.9×10^3 g mol^{-1} **(7c)**.

crystal morphology is mainly determined by the structure of the hard segment. For all copolymers, the L_c is found to be somewhat larger than the estimated hard block length, which indicates that the crystalline core in the copolymer structure also partially includes the ester groups.

When the length of the crystalline stem is calculated by dividing L_c by the cosine of the tilt angle, one can see that copolymers **7a** (glycine substituted bisoxalamide) and **8** (β-alanine substituted bisoxalamide) exhibit similar values of the stem length (~25 Å) while their melting temperatures, 119 °C and 142 °C, respectively, strongly differ. Therefore, the L_c is not the only parameter determining the melting temperature, but the arrangement of the hard block inside the unit cell (*i.e.* the chain tilt and possibly the difference in the H-bonding energy are also important).

3.4.4. Temperature-dependent WAXS/SAXS

Temperature-dependent WAXS and SAXS measurements were performed to obtain information on the evolution of the phase-separated morphology upon heating. Fig. 10 shows the results of such measurements for the segmented poly(ether ester amide)s with different soft segment lengths **(7a–c)**.

Below 0 °C, the (020) and (110) peaks of PTHF crystals are clearly seen for the copolymers with PTHF segment lengths of 2.0×10^3 and 2.9×10^3 g mol^{-1} (**7b** and **c**). Moreover, the PTHF peaks are much stronger for copolymer **7c**, indicating that the crystallinity of the soft block rapidly increases with its length. The melting transitions of PTHF crystals visible from the variation of the (020) and (110) peaks intensity are in agreement with DSC measurements. The main SAXS interference maximum and the form factor of the bisoxalamide crystals located at ~0.07 Å^{-1} disappear at the melting temperature of the copolymer hard blocks indicating a transition to the homogeneous melt.

3.5. Dynamic mechanical properties

Temperature dependent mechanical properties were studied using DMA and the storage modulus and loss modulus as a function of the temperature are depicted in Fig. 11. The glass transition temperatures range from −65 to −75 °C and correspond well to the glass transition temperatures measured by DSC. The crystallization of the polytetrahydrofuran with molecular weights of 2.0×10^3 and 2.9×10^3 g mol^{-1} is reflected by the presence of a shoulder in the storage modulus prior to the start of the rubber plateau. For all polymers, this plateau is broad and remains constant up to the flow temperature, which is typical for segmented block copolymers with uniform hard segments. By increasing the molecular weight of the polytetrahydrofuran, the storage modulus at 25 °C decreases from 54 to 12 MPa due to a decreasing hard segment content (Fig. 12a). Whereas PTHF$_{1000}$-Gly-OXA$_2$6-Gly **(7a)** has a storage modulus of 54 MPa, PTHF$_{1000}$-Gly-OXA$_2$2-Gly **(5)**, PTHF$_{1000}$-Gly-OXA$_2$4-Gly **(6)** and PTHF$_{1000}$-βAla-OXA$_2$6-βAla **(8)** have higher moduli in between 77 and 79 MPa. Possibly, the lower stiffness of polymer **7a** is due to the lower hard segment crystallinity as measured by FT-IR and DSC. When the hard segment starts to melt, the polymer softens and as a result the modulus drops. By increasing the soft segment M_n, the flow temperature decreases from 122 to 112 °C **(7a–c)**. Increasing the spacer length between the oxalamide groups from 2 to 6 methylene groups results in a decrease of the flow temperature from 170 to 122 °C. Changing the glycine ester into a β-alanine ester keeping the spacer length constant increases the flow temperature from 122 to 143 °C.

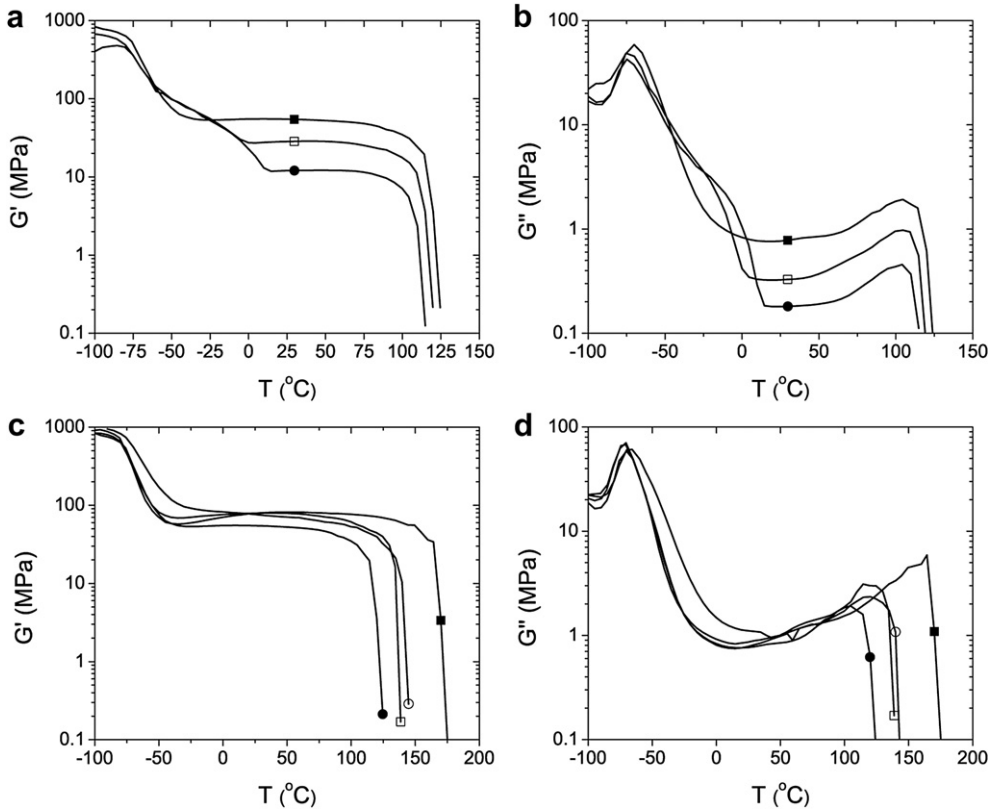

Fig. 11. Storage modulus (G′) and loss modulus (G″) as a function of temperature for segmented poly(ether ester amide)s (a–b) (■) PTHF$_{1000}$-Gly-OXA$_2$6-Gly **(7a)**, (□) PTHF$_{2000}$-Gly-OXA$_2$6-Gly **(7b)** and (●) PTHF$_{2900}$-Gly-OXA$_2$6-Gly **(7c)**.(c–d) (■) PTHF$_{1000}$-Gly-OXA$_2$2-Gly **(5)**, (□) PTHF$_{1000}$-Gly-OXA$_2$4-Gly **(6)**, (●) PTHF$_{1000}$-Gly-OXA$_2$6-Gly **(7a)** and (○) PTHF$_{1000}$-βAla-OXA$_2$6-βAla **(8)**.

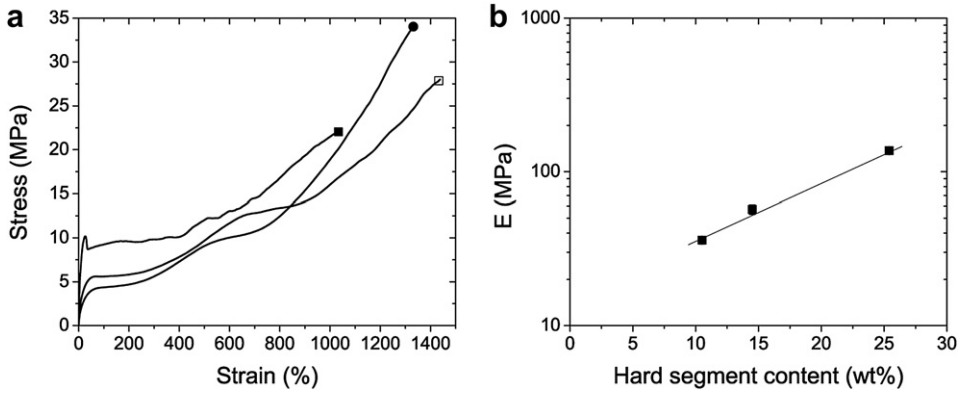

Fig. 12. (a) Stress–strain curves for segmented poly(ether ester amide)s (■) $PTHF_{1000}$-Gly-$OXA_2$6-Gly **(7a)**, (□) $PTHF_{2000}$-Gly-$OXA_2$6-Gly **(7b)** and (●) $PTHF_{2900}$-Gly-$OXA_2$6-Gly **(7c)**. (b) E-modulus as a function of hard segment content.

3.6. Mechanical properties

The mechanical properties of the segmented poly(ether ester amide)s were evaluated by tensile testing of dumbbells (ISO37 s2) cut from compression molded bars. Test data are collected in Table 5. Typical stress–strain curves are presented in Figs. 12 and 13.

For the deformation of segmented thermoplastic elastomers with uniform hard segments the following picture emerges from the literature [14,28]. Non-oriented samples consist of fiber-like nano-crystals randomly distributed in a soft polymer matrix. At low strains, below the yield point, the ***a***-axis of the crystals orient parallel to the stretching direction. At these low strains, hardly any orientation of the soft segment is observed. Above the yield point, a different deformation mechanism sets in. The crystals break up in smaller fragments and the ***a***-axis becomes oriented perpendicular to the stretching direction. Upon further elongation, the soft segments also orient in the direction of the deformation. Finally, the hard segment crystals prevent chain slippage of the soft segments and hence failure of the sample.

The E-modulus was determined at small deformations where the stress increases linearly with strain. The E-modulus of PTHF-Gly-$OXA_2$6-Gly **(7a–c)** increases as the soft segment M_n decreases and thus the hard segment content increases.

According to Wegner [41], the logarithm of the modulus of a segmented copolymer follows a linear relationship with crystalline volume fraction. Since the degrees of crystallinity of the hard phase in polymers **7a–c** are comparable and the density of the hard segment crystal is similar, the volume fraction is linear with the weight fraction. Plotting the logarithm of the E-modulus against the hard segment weight fraction confirms the linear relationship (Fig. 12b). Above the yield point, the material is permanently deformed. By increasing the polytetrahydrofuran molecular weight, the yield stress decreases and the yield strain increases. Polymer **7a** displays a distinct yield point whereas this is less pronounced for **7b–c**. A distinct yield point indicates a long-range hard segment connectivity and a well percolated hard phase throughout the soft polymer matrix [5,6]. The strain at break for all three polymers is higher than 1000%. The upsweep in the stress–strain curves at higher strains is caused by a strain hardening effect. For polymers **7b–c** the strain hardening effect may be caused by strain induced crystallization of the polytetrahydrofuran soft segments and as a result the stress at break is higher at increasing polytetrahydrofuran M_n. The stress–strain curves of the segmented poly(ether ester amide)s $PTHF_{1000}$-Gly-$OXA_2$6-Gly **(7a)** and PTHF1000-βAla-OXA26-βAla **(8)** are depicted in Fig. 13.

Both polymers show a pronounced yield point followed by necking and strain hardening. Interestingly, the copolymer with the β-alanine based hard segments **(8)** shows a more pronounced strain hardening effect than the copolymers with the glycine based hard segment **(7a)** and as a consequence the fracture stress of this polymer is higher. The glycine based segmented copolymers **5** and **6** reveal a similar strain hardening effect as copolymer **7a**. The difference observed in strain hardening is thought to be a result of the bisoxalamide crystal structure. At high strains, the fiber-like nano-crystals break up in smaller fragments and bisoxalamide hard segments become oriented parallel to the stretching direction. Moreover, the soft segment is also oriented in the tensile direction. The hard segment crystals prevent chain slippage of the soft segments and hence failure of the sample. Copolymer **7**, with the β-alanine based segment, shows more effective strain hardening compared to the glycine based copolymers **7a** suggesting more

Table 5
Mechanical properties of segmented poly(ether ester amide)s **5–8**.

	Content[a]		X_c[b] (%)	E (MPa)	σ_y (MPa)	ε_y (%)	σ_b (MPa)	ε_b (%)
	Soft segment (%)	Hard segment (%)						
7a	74.6	25.4	85	137 ± 7	10.2 ± 0.3	26 ± 1	22.2	1040
7b	85.5	14.5	95	57 ± 4	5.2 ± 0.1[c]	37±1[c]	28	1448
7c	89.5	10.5	99	36 ± 2	3.87 ± 0.1[c]	45±1[c]	34.1	1238
5	77.8	22.2	100	171 ± 2	13.0 ± 0.1	38 ± 1	19	890
6	76.2	23.8	100	161 ± 10	12.7 ± 0.1	34 ± 1	12.8	510
8	73.1	26.9	88	169 ± 4	13.9 ± 0.2	40 ± 1	30.9	850

[a] The ester groups are included in the calculation of the hard segment content.
[b] Degrees of crystallinity determined by DSC.
[c] Estimated from the intersect of tangents to stress-strain diagrams as the curves did not show a distinct yield point.

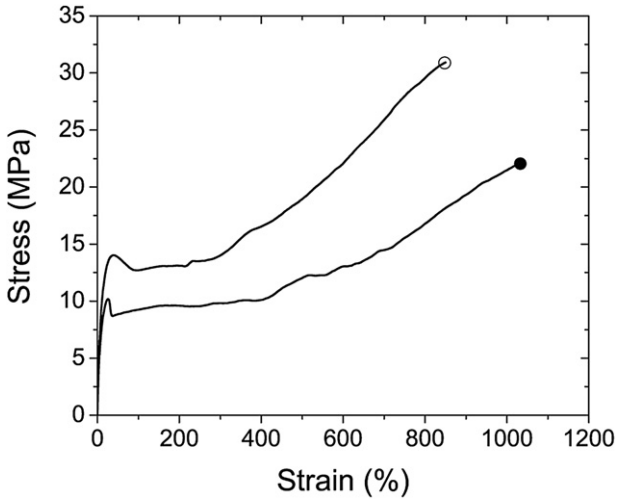

Fig. 13. Stress–strain curves of segmented poly(ether ester amide)s (●) $PTHF_{1000}$-Gly-$OXA_2$6-Gly **(7a)** and (○) $PTHF_{1000}$-βAla-$OXA_2$6-βAla **(8)**.

resistance of chain slippage and thus more resistance against disruption of the crystalline structure.

4. Conclusions

Novel 100% aliphatic thermoplastic elastomers are introduced based on oxalic acid chemistry and industrial and potentially renewable monomers like glycine (ethyl ester), aliphatic diamines and high molecular weight diols. In particular, segmented poly(-ether ester amide)s were prepared by melt polycondensation of α,ω-hydroxyl end functionalized polytetrahydrofuran and –OH reactive bisester–bisoxalamides with spacer lengths of 2, 4 or 6 methylene groups and capped with glycine- or β-alanine ethyl ester functional groups. The properties stem from the strong and directional H-bonding of the oxalamide unit. All segmented copolymers appear to be highly phase separated materials with a broad temperature independent rubber plateau starting at low temperatures. FT-IR revealed strongly hydrogen bonded and highly ordered bisoxalamide segments with hydrogen bonds formed between the oxalamide groups. The hard segment crystallinities were in between 73 and 99%. A fibrillar morphology consisting of ribbon-like nano-crystals randomly dispersed in the polyether matrix was observed using AFM. Further structural information was extracted from simultaneous small- and wide-angle X-ray scattering. The long dimension of the crystals is parallel to the direction of the hydrogen bonds, whereas the two small dimensions correspond to the length of one bisoxalamide segment and to the width of the stacks of hydrogen bonded sheets containing ca. 6 to 12 hydrogen bonded sheets, respectively. The melting transition of the glycine based hard segment increased from 119 to 170 °C with decreasing spacer length from 6 to 2 methylene groups. Moreover, changing the glycine ester group into a β-alanine ester group, Gly-$OXA_2$6-Gly to βAla-$OXA_2$6-βAla, led to an increase of the melting transition of the hard segments from 119 to 141 °C. The polymers show an elastic modulus in a range between 139 and 170 MPa with yield stresses between the 10.2 and 13.9 MPa and strains at break higher than 800%. Whereas the fracture stress of the β-alanine based segmented poly(ether ester amide) was 31 MPa, the fracture stress of the glycine based copolymers was not higher than 22 MPa. The differences in thermal and mechanical properties between the copolymers comprising β-alanine or glycine based hard segments is related to a difference in the crystal structure of the hard segment.

Acknowledgements

We thank Hetty ten Hoopen for the AFM measurements. This research was financially supported by the Dow chemical company under research agreement 218193. MR, YO and DAI acknowledge the French Agence Nationale de la Recherche (SPIRWIND project of the HABISOL program and T2T project of the Blanc International program) for financial support. The authors are also grateful to Wim Bras and Giuseppe Portale from the DUBBLE beamline (ESRF, France) for fruitful discussions and excellent technical support.

Appendix A. Supplementary information

Supplementary data related to this article can be found online at http://dx.doi.org/10.1016/j.polymer.2012.07.015.

References

[1] Fakirov S. Handbook of condensation thermoplastic elastomers. Weinheim: Wiley-VCH; 2005.
[2] Holden G, Legge NR, Quirk RP, Schroeder HE. Thermoplastic elastomers. 2nd ed. Munich: Hanser Publishers; 1996.
[3] Cella RJ. J Polym Sci Symp No 47 1973;42:727–40.
[4] Biemond GJE, Feijen J, Gaymans RJ. Polym Eng Sci 2008;48:1389–400.
[5] Das S, Cox DF, Wilkes GL, Klinedinst DB, Yilgor I, Yilgor E, et al. J Macromol Sci Phys 2007;46:853–75.
[6] Das S, Yilgor I, Yilgor E, Inci B, Tezgel O, Beyer FL, et al. Polymer 2007;48:290–301.
[7] Eisenbach CD, Stadler E. Macromol Chem Phys 1995;196:1981–97.
[8] Fu B, Macknight WJ, Schneider NS. Rubber Chem Technol 1986;59:896–911.
[9] Harrell LL. Macromolecules 1969;2:607–12.
[10] Miller JA, Lin SB, Hwang KKS, Wu KS, Gibson PE, Cooper SL. Macromolecules 1985;18:32–44.
[11] Ng HN, Allegrez AE, Seymour RW, Cooper SL. Polymer 1973;14:255–61.
[12] Niesten MCEJ, Feijen J, Gaymans RJ. Polymer 2000;41(24):8487–500.
[13] Shirasaka H, Inoue S, Asai K, Okamoto H. Macromolecules 2000;33:2776–8.
[14] Versteegen RM, Kleppinger R, Sijbesma RP, Meijer EW. Macromolecules 2006;39:772–83.
[15] Versteegen RM, Sijbesma RP, Meijer EW. Macromolecules 2005;38:3176–84.
[16] Yilgor I, Shaaban AK, Steckle WP, Tyagi D, Wilkes GL, McGrath JE. Polymer 1984;25:1800–6.
[17] Yilgor I, Yilgor E. Polym Rev 2007;47:487–510.
[18] Tyagi D, Yilgor I, McGrath JE, Wilkes GL. Polymer 1984;25:1807–16.
[19] Arun A, Gaymans RJ. Macromol Chem Phys 2008;209:854–63.
[20] Biemond GJE, Feijen J, Gaymans RJ. J Appl Polym Sci 2007;105:951–63.
[21] Bouma K, Wester GA, Gaymans RJ. J Appl Polym Sci 2001;80:1173–80.
[22] Gaymans RJ, Dehaan JL. Polymer 1993;34:4360–4.
[23] Husken D, Feijen J, Gaymans RJ. J Polym Sci Part A Polym Chem 2007;45:4522–35.
[24] Krijgsman J, Husken D, Gaymans RJ. Polymer 2003;44:7573–88.
[25] Krijgsman J, Husken D, Gaymans RJ. Polymer 2003;44:7043–53.
[26] Niesten MCEJ, Bouma K, Gaymans RJ. Polymer 1998;39:93–8.
[27] Niesten MCEJ, Gaymans RJ. Polymer 2001;42:6199–207.
[28] Niesten MCEJ, Harkema S, van der Heide E, Gaymans RJ. Polymer 2001;42:1131–42.
[29] Niesten MCEJ, Tol R, Gaymans RJ. Polymer 2001;42:931–9.
[30] van der Schuur M, de Boer J, Gaymans RJ. Polymer 2005;46:9243–56.
[31] van der Schuur M, Feijen J, Gaymans RJ. Polymer 2005;46:4584–95.
[32] van der Schuur M, Feijen J, Gaymans RJ. Polymer 2005;46:327–33.
[33] Van der Schuur M, Gaymans RJ. J Polym Sci Part A Polym Chem 2006;44:4769–81.
[34] Sijbrandi NJ, Kimenai AJ, Mes EPC, Broos R, Bar G, Rosenthal M, et al. Macromolecules 2012;45:3948–61.
[35] Meier RJ. Vib Spectrosc 2005;39:266–9.
[36] Asin L, Armelin E, Montane J, Rodriguez-Galan A, Puiggali J. J Polym Sci Part A Polym Chem 2001;39:4283–93.
[37] Flory PJ. Trans Faraday Soc 1955;51:848–57.
[38] Ivanov DA, Hocquet S, Dosiere M, Koch MHJ. Eur Phys J E 2004;13:363–78.
[39] Ivanov DA, Bar G, Dosiere M, Koch MHJ. Macromolecules 2008;41:9224–33.
[40] De ten Hove CLF, Penelle J, Ivanov DA, Jonas AM. Nat Mater 2004;3:33–7.
[41] Legge NR, Holden G, Schroeder HE. Thermoplastic elastomers: a comprehensive review, 1ed. Munich: Hanser; 1987.